# Optical Field Transmission Analysis of an All-Fiber Signal Combiner With a Dumbbell Shape

Xuanfeng Zhou

***Abstract*—In this paper, the optical field transmission characteristics of an all-fiber signal combiner with a dumbbell shape and its application in laser beam combining are analyzed theoretically. Based on the three-layer waveguide model, the mode characteristics of a tapered multi-core fiber and a tapered single core fiber are analyzed respectively. On this basis, the working principle of an all-fiber signal combiner with a dumbbell shape is introduced from the perspective of mode evolution. The finite-difference beam propagation method is used to numerically analyze optical field envolution process in the combiner. Influences of the waist diameter, taper length and geometric arrangement are analyzed in detail. The calculation results show that an all-fiber signal combiner with a dumbbell shape can realize high brightness laser beam combining and the beam quality can reach the theoretical limit.**

***Index Terms*—Fiber laser, laser beam combining, fiber combiner, beam quality.**

## I. Introduction

FIBER laser has the advantages of high conversion efficiency, good beam quality, compact structure and convenient maintenance, which has been widely used in many fields such as scientific research, industrial manufacturing and defense security [1], [2], [3]. With the improvement of pump source brightness and fiber manufacturing craft, the output power of the fiber laser has been rapidly developed in this century and has become an important research direction of high-power lasers [4]–[5]. At present, the output power of a single-mode fiber laser has exceeded 10 kilowatts [6]. However, there are many challenges to further improve the output power of a single fiber laser [7]–[8]. To solve this problem, laser beam combining is supposed to be an effective method to further improve the output power [9], [10], [11]. Fiber combiner is an all-fiber device that can combine multiple fiber laser s into one fiber for output. It is one of the most important solutions to break the output power bottleneck of a single fiber laser [12], [13], [14], [15].

The traditional all-fiber signal combiner is obtained by tapering and cutting the input fiber bundle to directly splice with the output fiber. This manufacturing process is relatively simple. The size of input fiber bundle is large and the size of output fiber is small, which can be seen as a pyramid shape. In order to maintain high transmission efficiency, the core diameter and numerical aperture of the output fiber cannot be too small, which means the number of modes in the output fiber is large and the beam quality of the output laser is poor. According to the reported experimental results, the brightness degradation of high-power combined laser based on all-fiber signal combiner is more than 30%. Correspondingly, if the output fiber with small core diameter and small numerical aperture is selected, the fiber combiner can be seen as a photonic lantern. In this condition, only a few modes are supported in the output fiber. However, photonic lantern cannot be applied to work in high-power scenarios due to its relatively low transmission effeciency [16]–[17].

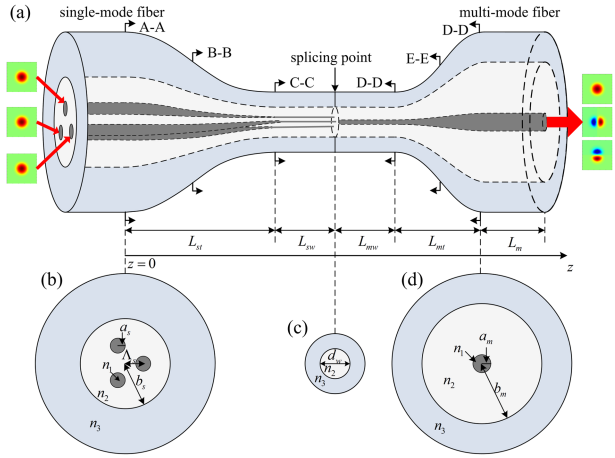


Fig. 1. Basic structure profile of an AFSCDS.

Based on the traditional all-fiber signal combiner and photonic lantern, an all-fiber signal combiner with a dumbbell shape (AFSCDS) is proposed in this paper. Its greastst feature is that a tapered double cladding fiber is used as the output fiber, the transmission efficiency is ensured by the inner cladding structure which can support a large number of modes. The beam quality is controlled by the core structure which can support only a few modes. Numerical simulation results show that an AFSCDS can realize high power and high brightness output laser in laser beam combining application.

## II. Theoretical Model

### A. Basic Structure of an AFSCDS

The basic structure of an AFSCDS is shown in Fig. 1(a). Fig. 1(b)–(d) show the cross-sectional profiles of the AFSCDS

Manuscript received 19 August 2022; revised 3 October 2022; accepted 4 October 2022. Date of publication 10 October 2022; date of current version 14 October 2022. This work was supported by the National Nature Science Foundation of China under Grant 11904398.

The author is with the State Key Laboratory of Complex Electromagnetic Environment Effects on Electronics and Information System Luoyang, Henan 471003, China (e-mail: zhouxuanfeng1988@163.com).

Digital Object Identifier 10.1109/JPHOT.2022.3213058

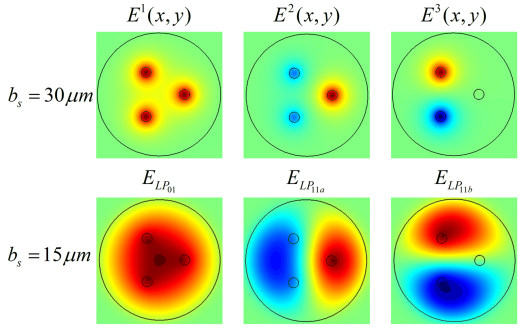


Fig. 2. Mode field distribution of isometric distributed three core fiber.

at different longitude positions. It can be seen from the figures that each cross-section includes three-layer structure with core, cladding and capillary, where the corresponding refractive index is defined as $n_1$, $n_2$ and $n_3$ respectively. In the longitude direction, the combiner mainly includes two parts: input single-mode fiber and output multi-mode fiber. Among them, the input single-mode fiber includes the original single-mode fiber, the taper region single-mode fiber and the taper waist single-mode fiber, and the output multi-mode fiber includes the original multi-mode fiber, the taper region multi-mode fiber and the taper waist multi-mode fiber. The taper waist single-mode fiber and the taper waist multi-mode fiber are connected through a splicing joint with equal cladding diameters. As shown in the figure, the core and cladding radii of the original single-mode fiber are defined $a_s$ as and $b_s$, and the distance from the core to the center is $\Lambda_s$. The core and cladding radii of the original multi-mode fiber are defined as $a_m$ and $b_m$. The cladding diameter at the splicing point is defined as $d_w$. The length of fiber in the taper region is $L_t$ ($L_{st}$ for single-mode fiber and $L_{mt}$ for multi-mode fiber), and that in the taper waist is $L_w$ ($L_{sw}$ for single-mode fiber and $L_{mw}$ for multi-mode fiber). The subscripts s and m are used to distinguish paremeters of single-mode fiber and multi-mode fiber.

The fabrication process of AFSCDS can be divided into the following three steps: 1) The original single-mode fiber is bundled with low refractive index capillary, and the fiber bundle is tapered to a proper size for cutting; 2) Insert the original multimode fiber into the low refractive index capillary, and taper the fiber and capillary to the proper size for cutting; 3) The input single-mode fiber and the output multi-mode fiber are spliced at the taper waist.

According to the above introduction, the analysis of AFSCDS mainly includes input single-mode fiber and output multi-mode fiber. As for the input single-mode fiber, since the multi-core structure will be formed after multiple single-mode fibers are bundled, it can be regarded as a tapered multi-core fiber. For the output multimode fiber, it can be simply regarded as a tapered single core fiber. It should be noted that since the influence of the original core at the splicing point can be ignored, and the waveguide formed by the cladding and the low refractive index capillary is the transmission channel of the optical field, the three-layer waveguide model should be used for the analysis of these two tapered fibers.

### B. Mode Characteristics of a Tapered Multicore Fiber

In the oringinal single-mode fiber, optical field is mainly transmitted in each core. As the size of the fiber decreases, the coupling between the cores will gradually increase. At this time, the mode of the fiber can be described by supermode. Due to the weakly guiding approximation, the polarization characteristic of the mode can be neglected, and the scalar form of multi-core fiber supermode can be obtained. Taking the isometric distributed three core fiber as an example, its electric field can be written as:

$$\begin{aligned} E^1(x,y,z) &= \frac{1}{\sqrt{3}}\left[E_1(x,y)\right. \\ &\quad \left. + E_2(x,y) + E_3(x,y)\right]\exp\left[i(\beta+2\kappa)z\right] \\ E^2(x,y,z) &= \frac{1}{\sqrt{6}}\left[2E_1(x,y)\right. \\ &\quad \left. - E_2(x,y) - E_3(x,y)\right]\exp\left[i(\beta-\kappa)z\right] \\ E^3(x,y,z) &= \frac{1}{\sqrt{2}}\left[E_2(x,y) - E_3(x,y)\right]\exp\left[i(\beta-\kappa)z\right] \end{aligned} \quad (1)$$

where $E^i$ (i = 1-3) is the electric field of multi-core fiber supermode, $E_i$ (i = 1-3) is the electric field of each core when mode coupling does not occur, $\beta$ is the corresponding propagation constant, $\kappa$ is the coupling coefficient between the cores.

It can be seen from (1) that when each core is a single-mode fiber, there are three supermodes corresponding to the three core fiber, wherein $E^2$ and $E^3$ have the same propagation constant, which means they are degenerate. COMSOL multiphysics software is used to solve the mode of three core fiber, and the mode field distribution is shown in Fig. 2. The basic parameters of the first row corresponding to the three core fiber are: core radius $a_s = 2.5\ \mu$m, core numerical aperture $NA_1 = 0.08$, distance from the core to the center $\Lambda_s = 12.5\ \mu$m, cladding radius is $b_s = 30\ \mu$m, cladding numerical aperture NA2 = 0.15. It should be pointed out that since the electric field obtained by COMSOL multiphysics software is the solution in vector form, Fig. 2 shows its component form in the x direction. The second row in Fig. 2 shows that COMSOL multiphysics software is used to calculate smaller size ($b_s = 15\ \mu$m) and the mode field distribution of the multi-core fiber is obtained. It can be seen from the figure that the influence of the core is very small, and the optical field is mainly distributed in the entire cladding area.

By changing the cross-sectional size, the mode effective refractive index ($n_{eff}$) corresponding to the tapered multi-core fiber at different positions can be solved, as shown in Fig. 3(a). The refractive indices of the core modes of the tapered multi-core fiber are basically the same when the cores are relatively large. With the gradual decrease of the core size, the core modes are gradually separated into $LP_01$ and $LP_{11}$ modes. When the effective refractive index of the mode is lower than the cladding refractive index (1.444), the mode is defined as the cladding mode. Therefore, in the propagation process of tapered multi-core fiber, optical field will gradually evolve from the core mode to the cladding mode.

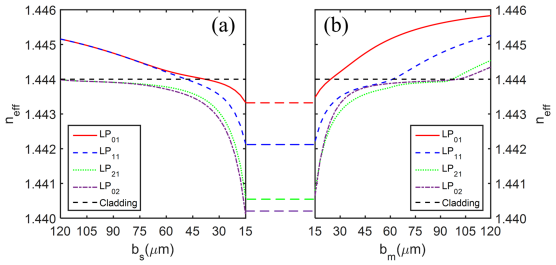


Fig. 3. Mode effective refractive index of a tapered fiber at different positions.

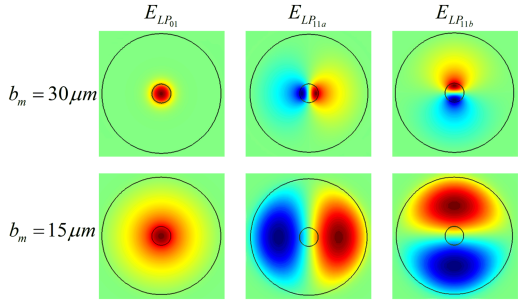


Fig. 4. Mode field distribution of isometric distributed three core fiber.

### C. Mode Characteristics of a Tapered Single Core Fiber

In the output multimode fiber, it can be regarded as a tapered single core fiber, and its analysis should be based on the three-layer waveguide model. When the weakly guiding approximation is adopted, the mode field distribution of the fiber can be expressed as linear polarization. The electric field corresponding to the LPmn mode (m is the angular ordinal number and n is the radial ordinal number) can be expressed as:

$$\begin{aligned}
\Psi_{mn} &= A_{mn} J_m\left(U_{mn}\frac{r}{a}\right)\begin{pmatrix}\cos(m\theta)\\ \sin(m\theta)\end{pmatrix} \quad r < a \\
\Psi_{mn} &= \left[B_{mn} I_m\left(W_{mn}\frac{r}{a}\right) + C_{mn} K_m\left(W_{mn}\frac{r}{a}\right)\right] \\
&\quad \times \begin{pmatrix}\cos(m\theta)\\ \sin(m\theta)\end{pmatrix} n_{eff} \geq n_2 \quad a \leq r \leq b \\
\Psi_{mn} &= \left[B_{mn} J_m\left(Q_{mn}\frac{r}{b}\right) + C_{mn} N_m\left(Q_{mn}\frac{r}{b}\right)\right] \\
&\quad \times \begin{pmatrix}\cos(m\theta)\\ \sin(m\theta)\end{pmatrix} n_{eff} < n_2 \quad a \leq r \leq b \\
\Psi_{mn} &= D_{mn} K_m\left(T_{mn}\frac{r}{b}\right)\begin{pmatrix}\cos(m\theta)\\ \sin(m\theta)\end{pmatrix} \quad r > b
\end{aligned} \tag{2}$$

where, A, B, C and D are coeffiencient constants, $J_m$ and $N_m$ are the m-order Bessel functions of the first and second kind respectively, $I_m$ and $K_m$ are the m-order modified Bessel functions of the first and second kind respectively, $U = ak_0\sqrt{n_1^2 - n_{eff}^2}$, $W = ak_0\sqrt{n_{eff}^2 - n_2^2}$, $Q = bk_0\sqrt{n_2^2 - n_{eff}^2}$, $T = bk_0\sqrt{n_{eff}^2 - n_3^2}$ are the normalized constants of the fiber and neff is the effective refractive index.

The optical field of the local mode of the fiber can be solved by the scalar wave equation together with the solution on the continuity of $\psi$ and d$\psi$/dr at the boundary. Therefore, the boundary continuity conditions can be applied to the core mode and the cladding mode respectively.

For the core mode, the eigenvalue equation can be expressed as:

$$\begin{vmatrix}
J_m(U) & -I_m(W) & -K_m(W) & 0 \\
\frac{U}{a}J'_m(U) & -\frac{W}{a}I'_m(W) & -\frac{W}{a}K'_m(W) & 0 \\
0 & I_m(W\frac{b}{a}) & K_m(W\frac{b}{a}) & -K_m(T) \\
0 & \frac{W}{a}I'_m(W\frac{b}{a}) & \frac{W}{a}K'_m(W\frac{b}{a}) & -\frac{T}{b}K'_m(T)
\end{vmatrix} = 0 \tag{3}$$

For the cladding mode, its eigenvalue equation can be expressed as:

$$\begin{vmatrix}
J_m(U) & -J_m(Q\frac{a}{b}) & -N_m(Q\frac{a}{b}) & 0 \\
\frac{U}{a}J'_m(U) & -\frac{Q}{b}J'_m(Q\frac{a}{b}) & -\frac{Q}{b}N'_m(Q\frac{a}{b}) & 0 \\
0 & J_m(Q) & N_m(Q) & -K_m(T) \\
0 & \frac{Q}{b}J'_m(Q) & \frac{Q}{b}N'_m(Q) & -\frac{T}{b}K'_m(T)
\end{vmatrix} = 0 \tag{4}$$

Eq. (3) and (4) respectively give the eigenvalue equations of the core mode and cladding mode obtained by the three-layer waveguide model. After the effective refractive index is obtained, the expression of the entire electric field can be further given according to the relationship between each electric field component.

COMSOL multiphysics software can also be used to solve the mode of single-core fiber, and the mode field distribution is shown in Fig. 4. The basic parameters corresponding to the first row are: core radius $a_m = 2.5$ $\mu$m, core numerical aperture $NA_1 = 0.08$, cladding radius $b_m = 30$ $\mu$m, cladding numerical aperture $NA_2 = 0.15$. It can be seen from the figure that the mode field of $LP_{01}$ mode is mainly distributed in the core area, while the mode field of $LP_{11}$ mode has gradually spread to the cladding area. The second row in Fig. 4 shows the mode field distribution of the single core fiber with smaller size ($b_m = 15$ $\mu$m). It can be seen from the figure the influence of the core is very small, and the optical field is mainly distributed in the entire cladding area.

By changing the cross-sectional size, the mode effective refractive index of the tapered single core fiber at different positions can also be obtained, as shown in Fig. 3(b). It can be seen that the refractive indices of different modes of tapered single core fiber are different in the whole range, so it can be considered that each mode can evolve independently. The mode in which the effective refractive index is lower than the cladding refractive index is also defined as the cladding mode. Therefore, in the propagation process of the tapered single core fiber, optical field will gradually evolve from the core mode to the cladding mode.

### D. Working Principle of an AFSCDS

For an AFSCDS, when a single laser beam is injected into the combiner from any core of the input single-mode fiber, it

will gradually excite the supermode in the multi-core fiber, and then evolve into the cladding mode in the taper waist single-mode fiber. Because the single-mode fiber and the multi-mode fiber at the taper waist have the same cladding structure, the cladding mode can be well matched at the splicing point. In the output multimode fiber, the cladding mode will evolve into the corresponding core mode with the increasing of core size, and will eventually be transmitted in the core of the multimode fiber. If multiple laser s are injected into the cores of the input single-mode fiber at the same time, the combined laser in the multi-mode fiber can be realized.

Here, the evolution process of optical field is explained by taking a 3 × 1 AFSCDS as an example. According to (1), supermodes in three core fiber and corresponding LP modes in multimode fiber can be obtained with different laser injection:

$$
\begin{aligned}
E_{Core-1} &= \begin{bmatrix} 1 \\ 0 \\ 0 \end{bmatrix} = \frac{1}{\sqrt{3}}E^1 + \frac{\sqrt{2}}{\sqrt{3}}E^2 \\
&= \frac{1}{\sqrt{3}}E_{LP_{01}}\mathrm{e}^{i\beta_{01}z} + \frac{\sqrt{2}}{\sqrt{3}}E_{LP_{11a}}\mathrm{e}^{i\beta_{11a}z} \\
E_{Core-2} &= \begin{bmatrix} 0 \\ 1 \\ 0 \end{bmatrix} = \frac{1}{\sqrt{3}}E^1 - \frac{1}{\sqrt{6}}E^2 + \frac{1}{\sqrt{2}}E^3 \\
&= \frac{1}{\sqrt{3}}E_{LP_{01}}\mathrm{e}^{i\beta_{01}z} - \frac{1}{\sqrt{6}}E_{LP_{11a}}\mathrm{e}^{i\beta_{11a}z} + \frac{1}{\sqrt{2}}E_{LP_{11b}}\mathrm{e}^{i\beta_{11b}z} \\
E_{Core-3} &= \begin{bmatrix} 0 \\ 0 \\ 1 \end{bmatrix} = \frac{1}{\sqrt{3}}E^1 - \frac{1}{\sqrt{6}}E^2 - \frac{1}{\sqrt{2}}E^3 \\
&= \frac{1}{\sqrt{3}}E_{LP_{01}}\mathrm{e}^{i\beta_{01}z} - \frac{1}{\sqrt{6}}E_{LP_{11a}}\mathrm{e}^{i\beta_{11a}z} - \frac{1}{\sqrt{2}}E_{LP_{11b}}\mathrm{e}^{i\beta_{11b}z}
\end{aligned}
\tag{5}
$$

where, $E_{LPmn}$ is the electric field of LPmn mode, $\beta_{01}$, $\beta_{11a}$ and $\beta_{11b}$ are the effective propagation constants of the corresponding modes, respectively.

Eq. (5) reflects the process of exciting the LP mode in cladding after laser is injected from each core, corresponding to the stage of core mode separation in Fig. 3(a). After that, independent propagation can be realized among various modes. The whole mode evolution process of the optical field in the AFSCDS can be seen from Fig. 5, where A-A∼F-F refer to the corresponding positions marked in Fig. 1.

It should be noted that the above analysis is based on local mode theory. For tapered fibers, adiabaticity criteria should be satisfied to achieve high-efficiency excitation of local modes [18]. That is, the change of tapered structure is slow enough to keep the optical field in the corresponding mode without exciting other modes. Generally speaking, adiabaticity criteria means the taper region of the tapered fiber should to be long enough, which is also a problem that needs to be solved in the practical application process.

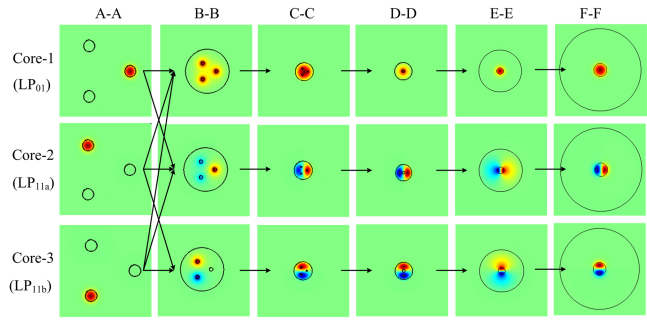


Fig. 5. Schematic diagram of mode evolution in an AFSCDS.

## III. Numerical Simulation

### A. Simulation of a 3 × 1 AFSCDS

Firstly, the finite-difference beam propagation method is used to analyze a 3×1 AFSCDS (named AFSCDS-TCF-1), whose basic structure is shown in Fig. 1. The main parameters of input single-mode fiber are: $a_s = 5\ \mu$m, $b_s = 60\ \mu$m, $\Lambda_s = 25\ \mu$m, $L_{st} = 20$ mm, $L_{sw} = 10$ mm. The main parameters of output multimode fiber are: $a_m = 10\ \mu$m, $b_m = 60\ \mu$m, $L_{mt} = 20$ mm, $L_{mw} = 10$ mm. The refractive index of the cladding is $n_2 = 1.444$. Core numerical aperture is $NA_1 = 0.08$, and the cladding numerical aperture is $NA_2 = 0.15$. The cladding diameter at the splicing point is $d_w = 30\ \mu$m. The optical field profiles at different longitude positions for different laser injections are calculated as shown in Fig. 6, where z = 60 mm∼80 mm is the original multimode fiber. The first row and the second row in the figure respectively show the electric field amplitude distribution when Core 1 and Core 2 are separately injected. The third row shows the electric field amplitude distribution when Core 1-3 are simultaneously injected with the same phase and equal power laser s, and the fourth row shows the electric field intensity distribution when Core 1-3 are simultaneously injected with equal power incoherent laser s. It can be seen from the figure that in the output multimode fiber, most of the combined laser is confined to the core for transmission. The total transmission efficiency of the combined laser is $T_{all} = 99.8\%$, in which the core mode accounts for $\eta_{core} = 88.6\%$, hence the transmission efficiency of the corresponding core mode laser is $T_{core} = T_{all} \times \eta_{core} = 88.4\%$.

According to the optical field distribution of the combined laser, the beam quality at different positions can be calculated, with the results shown in Fig. 7(a). It can be seen that at the taper region of single-mode fiber, the $M^2$ factor of the combined laser continuously decreases. When reaching the taper waist region, the beam quality of the coherent combined laser is $M^2 = 1.2$, and the beam quality of the incoherent combined laser is $M^2 = 1.9$. At the splicing point, the $M^2$ factor of the combined laser suddenly changes. Finally, the beam qualities of coherent and incoherent combined laser in the output multimode fiber are $M^2 = 2.83$ and $M^2 = 3.32$ respectively. The fluctuation of $M^2$ factor is mainly caused by the influence of cladding mode. For core mode laser, the beam qualities of coherent and incoherent

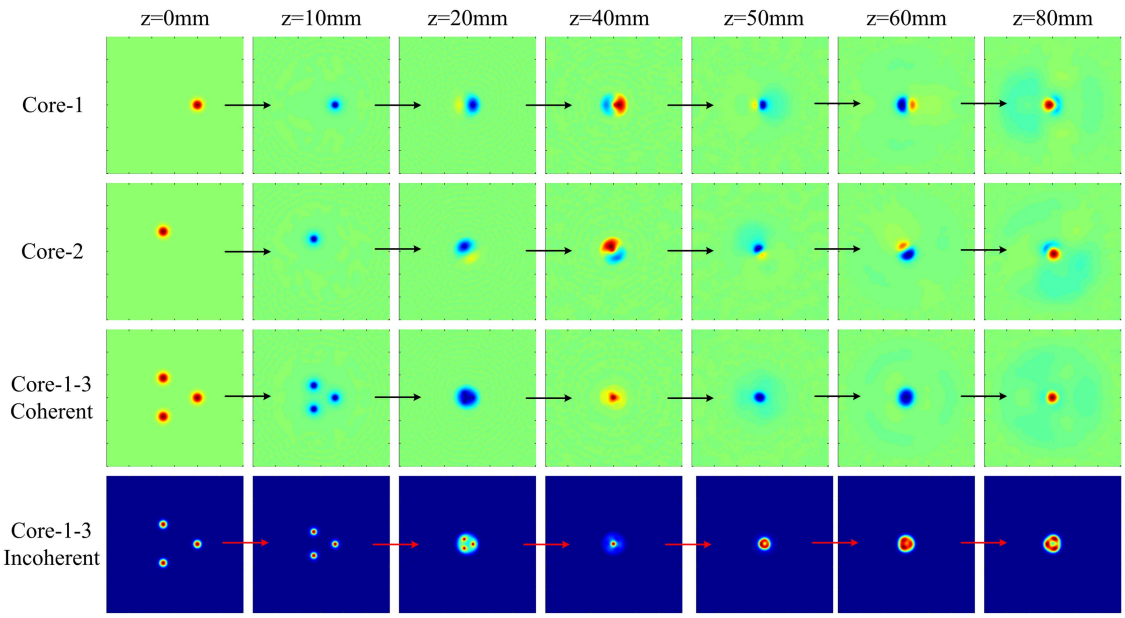


Fig. 6. Optical field evolution progress at different longitude positions in a 3 × 1 AFSCDS.

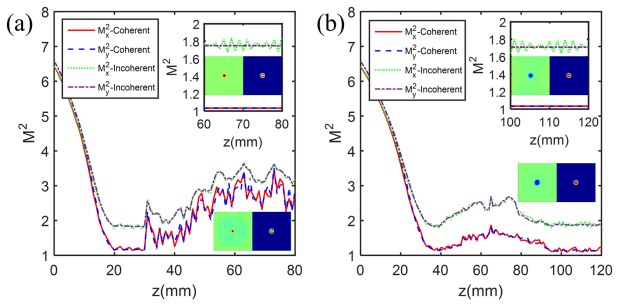


Fig. 7. Beam quality ($M^2$ factor) evolution process at different longitude positions in a 3 × 1 AFSCDS.

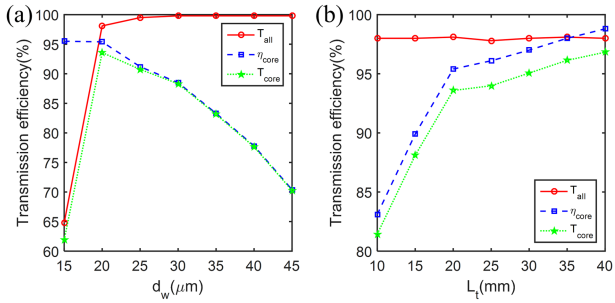


Fig. 8. Transmission efficiency of a 3 × 1 AFSCDS for different taper waist diameters (a) and taper lengths (b).

combined laser in the output multimode fiber are $M^2 = 1.03$ and $M^2 = 1.75$ respectively, as shown in the inset in Fig. 7(a). Hence, it can be seen that the output laser beam quality can reach the theoretical limit when the AFSCDS is used for fiber laser beam combining [19].

In order to further improve the transmission efficiency of core mode laser, the influence of the waist diameter $d_w$ and the taper length $L_t$ are investigated respectively, with the results shown in Fig. 8. In Fig. 8(a), the taper length is fixed with $L_t = 20$ mm. It can be seen from the figure that the total transmission efficiency of the combined laser Tall gradually increases with $d_w$. This is because the mode capacity of the inner cladding structure at the taper waist is increasing. However, the proportion of the core mode in the combined laser $\eta$core is gradually decreasing because there are more cladding modes at the taper waist that cannot be coupled back to the core. Considering the two factors, the transmission efficiency of the core mode laser Tcore reaches the maximum for $d_w = 20$ $\mu$m. In Fig. 8(b), the waist diameter is fixed with $d_w = 20$ $\mu$m. It can be seen from the figure that the total transmission efficiency of the combined laser Tall is basically the same, while the proportion of the core mode in the combined laser $\eta$core is gradually increasing, which makes the transmission efficiency of core mode laser Tcore gradually increasing.

Beam quality at different longitude positions of the beam combiner is calculated for $d_w = 20$ $\mu$m and $L_t = 40$ mm (named AFSCDS-TCF-2), with the results are shown in Fig. 7(b). It can be seen from the figure that the beam qualities of coherent and incoherent combined laser in the output multimode fiber are $M^2 = 1.14$ and $M^2 = 1.89$. For core mode laser, the beam qualities of coherent and incoherent combined laser in the output multimode fiber are $M^2 = 1.03$ and $M^2 = 1.72$, respectively. It can be seen that, when the parameters of the beam combiner are properly selected, the combined laser is mainly transmitted in the fiber core, and the high-power combined laser can be obtained either in the core or in the whole fiber structure.

### *B. Simulation of a 7 × 1 AFSCDS*

Next, the beam propagation method is also used for analyzing a 7×1 AFSCDS (named AFSCDS-ECF-1). The main

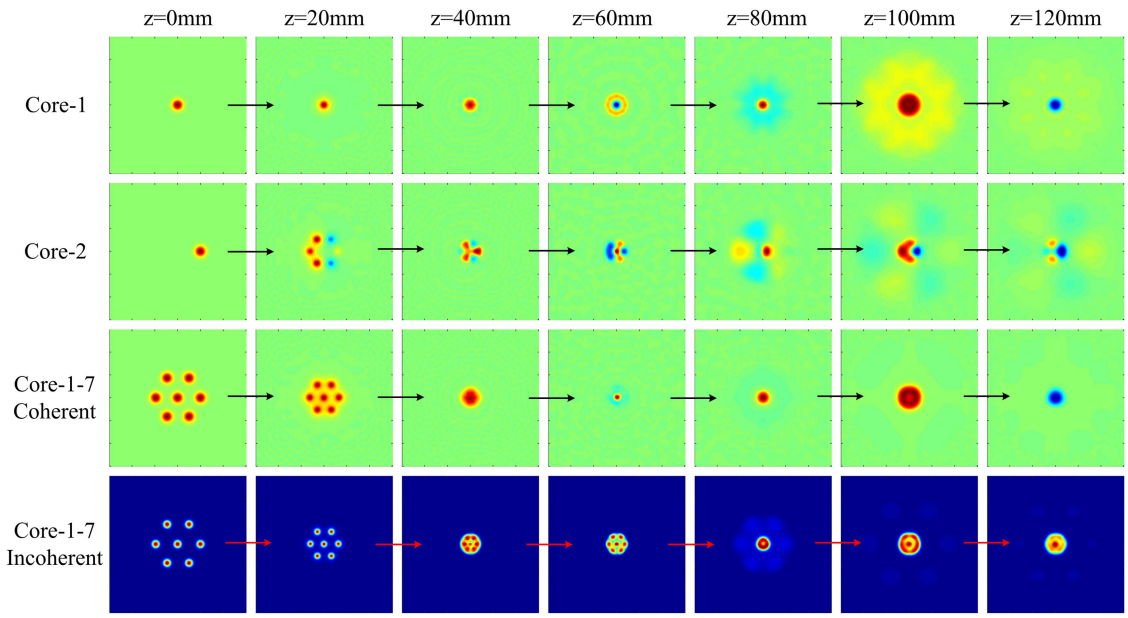


Fig. 9. Optical field evolution progress at different longitude positions in a 7 × 1 AFSCDS.

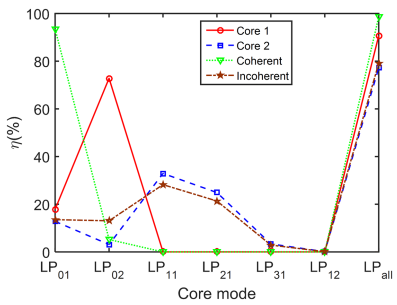


Fig. 10. Mode content in output laser of a 7 × 1 AFSCDS.

parameters of input single-mode fiber are the same with AFSCDS-TCF-2. In order to increase the mode capacity of the core, the core radius of the output multimode fiber is increased to $a_m = 12.5\ \mu m$. The taper length is set as $L_t = 40$ mm, and the cladding diameter at the splicing point is $d_w = 25\ \mu m$. The optical field profiles at different longitude positions for different laser injections are calculated as shown in Fig. 9. The total transmission efficiency of the combined laser is $T_{all} = 99.1\%$, and the transmission efficiency of the core mode laser is $T_{core} = 77.6\%$. The beam qualities of coherent and incoherent combined laser in the output multimode fiber are $M^2 = 1.42$ and $M^2 = 5.03$. For core mode laser, the beam qualities of coherent and incoherent combined laser in the output multimode fiber are $M^2 = 1.18$ and $M^2 = 2.40$, respectively. From the perspective of core mode laser, it can be seen that the output laser beam quality can reach or even surpass the theoretical limit [19].

According to the optical field information obtained by simulation calculation, the optical field in the output fiber is mode decomposed, with the results shown in Fig. 10. It can be seen from the figure that Core 1 only excites LP0n mode, while Core 2 excites all LP modes. For coherent combining case, only $LP_{01}$ mode and a small amount of $LP_{02}$ mode are excited, so near-diffraction-limit combined laser can be obtained. For incoherent combining case, the number of excited modes increase, and the beam quality of the combined laser becomes poor.

### C. Simulation of a 6 × 1 AFSCDS

Finally, the influence of geometric arrangement in input fiber is analyzed by numerical simulation of a 6×1 AFSCDS. In the case of six input single-mode fibers, there are mainly two knids of geometric arrangement methods: one is ring arrangement and the other is quasi-isometric arrangement. The former one has no center core (named AFSCDS-ICF-1), while the latter one has a center core (named AFSCDS-ICF-2). In the simulation, the main parameters of input single-mode fiber are the same with those of AFSCDS-ECF-1. The taper length is set as $L_t = 40$ mm, and the cladding diameter at the splicing point is $d_w = 25\ \mu m$. The optical field profiles at different longitude positions for different laser injections are calculated as shown in Fig. 11.

According to the optical field information obtained by simulation calculation, the optical field in the output fiber is mode decomposed, with the results shown in Fig. 12. Fig. 12(a) is the result of AFSCDS-ICF-1, and Fig. 12(b) is the result of AFSCDS-ICF-2. It can be seen from the figure that the Core 1 in AFSCDS-ICF-2 can only excite the LP0n mode because there is a center core for quasi-isometric arrangement. However, from the perspective of the combined laser, the ring arrangement is more suitable for coherent combining because more fundamental modes can be excited, and the quasi-isometric arrangement is more suitable for incoherent combining because more low-order modes can be excited.

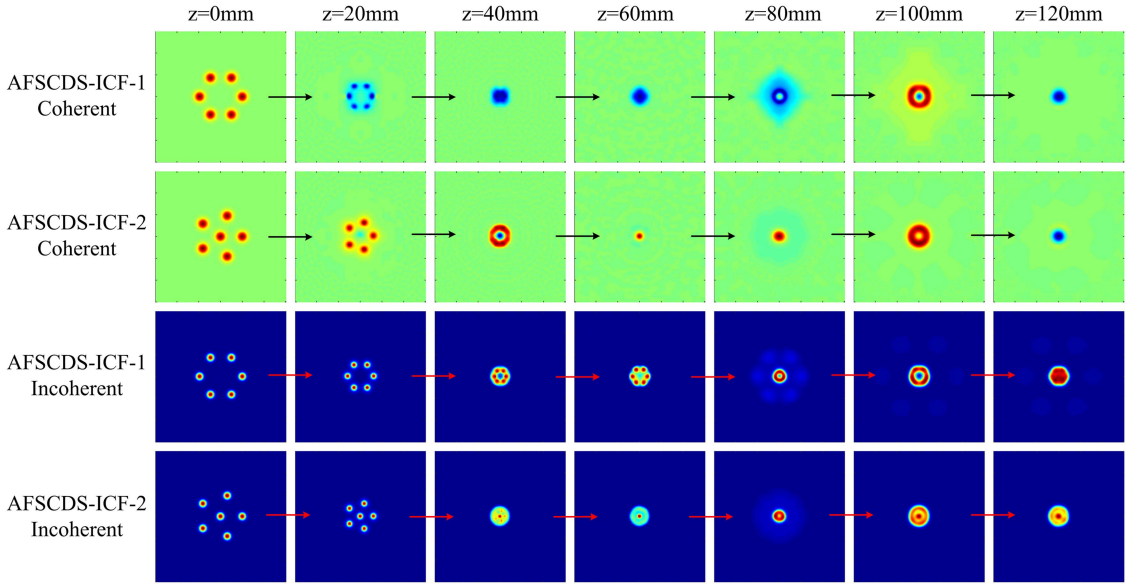


Fig. 11. Optical field evolution progress at different longitude positions in a 6 × 1 AFSCDS.

TABLE I
THIS IS A SAMPLE OF A TABLE TITLE

| Combiner | Input laser | | Transmission efficiency | | Coherent | | Incoherent combinging | |
|---|---|---|---|---|---|---|---|---|
| | $M_0^2$ | N | $T_{all}$(%) | $T_{core}$(%) | $M_N^2$ | RBr(%) | $M_N^2$ | RBr(%) |
| Ref. [12] | 1.29 | 7 | 98.0 | 98.0 | \ | \ | 4.30 | 61.7 |
| Ref. [13] | 1.30 | 7 | 98.5 | 98.5 | \ | \ | 5.37 | 40.4 |
| Ref. [14] | 1.92 | 3 | 99.0 | 99.0 | \ | \ | 6.00 | 30.4 |
| Ref. [15] | 1.27 | 4 | 96.0 | 96.0 | \ | \ | 4.03 | 38.1 |
| AFSCDS- | 1.02 | 3 | 99.8 | 88.4 | 1.03 | 260 | 1.76 | 89.0 |
| AFSCDS- | 1.02 | 3 | 98.1 | 96.9 | 1.03 | 285 | 1.72 | 102 |
| AFSCDS- | 1.02 | 7 | 99.1 | 77.6 | 1. | 406 | 2.40 | 98.1 |
| AFSCDS- | 1.02 | 6 | 99.1 | 78.0 | 1.24 | 317 | 2.32 | 90.4 |
| AFSCDS- | 1.02 | 6 | 97.7 | 88.7 | 1.53 | 236 | 2.34 | 101 |

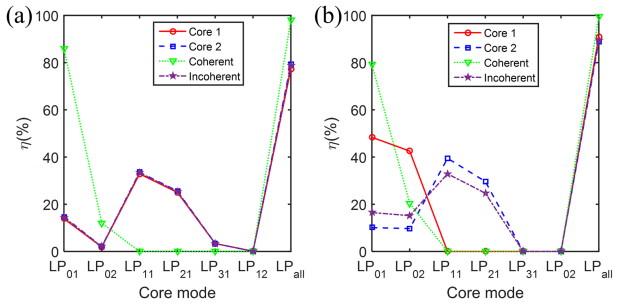


Fig. 12. Mode content in output laser of a 6 × 1 AFSCDS.

## D. Discussion

In this part, we mainly focus on the beam quality of combined laser. The brightness of a laser beam can be calculated by the optical power divided by the product of the focused beam mode area and the solid angel of divergence [20]:

$$Br = \frac{P}{A\Omega} \tag{6}$$

where P is the output power, A = $\pi\omega 2$ 0 is the focused beam mode area and $\Omega = \pi\theta^2$ is the solid angel of divergence.

$M^2$ factor is defined as:

$$M^2 = \frac{\omega_0 \theta}{\lambda/\pi} \tag{7}$$

Hence, the brightness of the laser beam can be expressed by $M^2$ factor:

$$Br = \frac{P}{(\lambda M^2)^2} \tag{8}$$

Here, a parameter named relative brightness is defined to describe the brightness change for laser beam combining:

$$RBr = \frac{Br_N}{Br_0} = TN\left(\frac{M_0^2}{M_N^2}\right)^2 \tag{9}$$

where $Br_N$ and $Br_0$ are the brightness of the combined laser and input laser, T is the transmission effeciency, M2 N and M2 0 are the beam quality of the combined laser and input laser.

Based on (9), relative brightness of ouput laser for beam combining based on fiber combiner is calculated, with results shown in Table I. For the experiment results in [12], [13], [14], [15], relative brightness is between 30.4%∼61.7%. It means laser brightness is degenerate due to the incoherent combining. For the simulation results in this work, both coherent combining and incoherent combining are calculated. In the coherent combining cases, brightnesses of combined laser are improved in all the simulation cases. However, brightness improvement is lower than the times of N, which is more obvious for cases with more input fibers. In the incoherent combining cases, brightnesses of combined laser are basically unchanged in all the simulation cases, which means laser brightness degeneration is not significant when the output power is improved

## IV. Conclusion

In this paper, an AFSCDS is introduced and its optical field transmission characteristics are analyzed theoretically. Firstly, the basic structure and fabrication process of an AFSCDS are introduced. Next, mode properties of the tapered multi-core fiber and tapered single core fiber are analyzed respectively. On this basis, the working principle of an AFSCDS is analyzed. Finally, AFSCDSs with $3 \times 1$, $7 \times 1$ and $6 \times 1$ are simulated by beam propagation method. The influence of different parameters on the optical field transmission characteristics of the combiner is also numerically analyzed. Theoretical analysis and numerical calculation show that an AFSCDS can optimize the laser beam quality with high-power laser output, and the laser beam quality can reach the theoretical limit, which has a great significance in beam combining of fiber laser.

## References


[1] A. Tünnermann, T. Schreiber, and J. Limpert, "Fiber laser s and amplifiers: An ultrafast performance evolution," *Appl. Opt.*, vol. 49, no. 25, pp. F71–F78, 2010.

[2] C. Jauregui, J. Limpert, and A. Tunnermann, "High-power fiber lasers," *Nature Photon.*, vol. 7, no. 11, pp. 861–867, 2013.

[3] M. N. Zervas and C. A. Codemard, "High power fiber lasers: A review," *IEEE J. Sel. Topics Quantum Electron.*, vol. 20, no. 5, pp. 219–241, Sep./Oct. 2014.

[4] Q. Fang et al., "5 kW near-diffraction-limited and 8 kW high-brightness monolithic continuous wave fiber lasers directly pumped by laser diodes," *IEEE Photon. J.*, vol. 9, no. 5, Oct. 2017, Art no. 1506107.

[5] L. Wang et al., "Theoretical and experimental study of high-peak-power high-brightness quasi-CW fiber laser," *IEEE Photon. J.*, vol. 14, no. 3, Jun. 2022, Art no. 1530206.

[6] B. Shiner, "The influence of fiber laser technology on the world wide material processing market," in *Proc. CLEO: Appl. Technol.*, 2013, p. AF2J.1.

[7] J. W. Dawson et al., "Analysis of the scalability of diffraction-limited fiber lasers and amplifiers to high average power," *Opt. Exp.*, vol. 16, no. 17, pp. 132401–13266, 2008.

[8] Y. Wen et al., "Experimental study on transverse mode instability characteristics of few-mode fiber laser amplifier under different bending conditions," *IEEE Photon. J.*, vol. 14, no. 4, Aug. 2022, Art no. 1539106.

[9] P. Ma et al., "7.1 kW coherent beam combining system based on a seven-channel fiber amplifier array," *Opt. Laser Technol.*, vol. 140, 2021, Art. no. 107016.

[10] J. Zuo et al., "Experimental demonstration of central-lobe energy enhancement based on amplitude modulation of beamlets in 19 elements fiber laser phased array," *IEEE Photon. J.*, vol. 13, no. 3, Jun. 2021, Art no. 1500113.

[11] Y. Yan et al., "Principle and numerical demonstration of high power all-fiber coherent beam combination based on self-imaging effect in a square core fiber," *Photon. Res.*, vol. 10, no. 2, pp. 444–455, 2022.

[12] X. Zhou, Z. Chen, Z. Wang, J. Hou, and X. Xu, "Beam quality analysis of incoherent beam combining by a $7 \times 1$ all-fiber signal combiner," *IEEE Photon. Technol. Lett.*, vol. 28, no. 20, pp. 2265–2268, Oct. 2016.

[13] C. Lei et al., "Incoherent beam combining of fiber lasers by an all-fiber $7\times1$ signal combiner at a power level of 14 kW," *Opt. Exp.*, vol. 26, no. 8, pp. 10421–10427, 2018.

[14] W. Wu, Z. Chen, Z. Wang, and J. Chen, "Beam combining of fiber lasers by a $3\times1$ signal combiner at a power $>$13 kW," *Opt. Fiber Technol.*, vol. 54, 2020, Art. no. 102109.

[15] F. Min, L. Zhixian, W. Zefeng, C. Zilun, and X. Xiaojun, "Research on a $4\times1$ fiber signal combiner with high beam quality at a power level of 12kW," *Opt. Exp.*, vol. 29, no. 17, pp. 26658–26668, 2021.

[16] J. Montoya et al., "Photonic lantern adaptive spatial mode control in LMA fiber amplifiers," *Opt. Exp.*, vol. 24, no. 4, pp. 3405–3413, 2016.

[17] J. Montoya, C. Hwang, D. Martz, C. Aleshire, T. Y. Fan, and D. J. Ripin, "Photonic lantern kW-class fiber amplifier," *Opt. Exp.*, vol. 25, no. 22, pp. 27543–27550, 2017.

[18] J. D. Love, W. M. Henry, W. J. Stewart, R. J. Black, S. Lacroix, and F. Gonthier, "Tapered single-mode fibres and devices: I. Adiabaticity criteria," *IEE Proc.*, vol. 138, no. 5, pp. 343–354, 1991.

[19] X. Zhou, D. Zhang, Y. Wang, W. Xiao, R. Zhu, and X. Men, "Beam quality analysis of output laser in a conventional photonic lantern excited by incoherent sources," in *Proc. SPIE*, vol. 11850, 2021, pp. 125–134.

[20] P. Shukla, J. Lawrence, and Y. Zhang, "Understanding laser beam brightness: A review and new prospective in material processing," *Opt. Laser Technol.*, vol. 75, pp. 40–51, 2015.